

## Article

# Dynamic Response of a Single-Rotor Wind Turbine with Planetary Speed Increaser and Counter-Rotating Electric Generator in Starting Transient State

Radu Saulescu <sup>1</sup>  and Mircea Neagoe <sup>2,\*</sup> 

<sup>1</sup> Design of Mechanical Elements and Systems R&D Centre, Faculty of Product Design and Environment, Transilvania University of Brasov, 500036 Brasov, Romania; rsaulescu@unitbv.ro

<sup>2</sup> Renewable Energy Systems and Recycling R&D Centre, Faculty of Product Design and Environment, Transilvania University of Brasov, 500036 Brasov, Romania

\* Correspondence: mneagoe@unitbv.ro; Tel.: +40-268-413-000

**Abstract:** The paper addresses the dynamic modeling and numerical simulation of a novel single-rotor wind system with a planetary speed increaser and counter-rotating direct current (DC) generator, patented by authors, during the transient stage from rest. The proposed analytical dynamic algorithm involves the decomposition of the wind system into its component rigid bodies, followed by the description of their dynamic equations using the Newton–Euler method. The linear mechanical characteristics of the DC generator and wind rotor are added to these dynamic equations. These equations allow for the establishment of the close-form equation of motion of the wind system and, implicitly, the time variation of the mechanical power parameters. Numerical simulations of the obtained analytical dynamic model were performed in MATLAB-Simulink in start-up mode from rest for the case study of a 100 kW wind turbine. These results allowed highlighting the time variation of angular velocities and accelerations, torques, and powers for all system shafts, both in the transient regime and steady-state. The implementation, in this case, of the counter-rotating generator indicates a 6.4% contribution of the mobile stator to the generator’s total power. The paper’s results are useful in the design, virtual prototyping, and optimization processes of modern wind energy conversion systems.



Academic Editor: Wei Huang

Received: 3 November 2024

Revised: 18 December 2024

Accepted: 25 December 2024

Published: 29 December 2024

**Citation:** Saulescu, R.; Neagoe, M. Dynamic Response of a Single-Rotor Wind Turbine with Planetary Speed Increaser and Counter-Rotating Electric Generator in Starting Transient State. *Appl. Sci.* **2025**, *15*, 191. <https://doi.org/10.3390/app15010191>

**Copyright:** © 2024 by the authors. Licensee MDPI, Basel, Switzerland. This article is an open access article distributed under the terms and conditions of the Creative Commons Attribution (CC BY) license (<https://creativecommons.org/licenses/by/4.0/>).

**Keywords:** renewable energy; wind turbines; counter-rotating electric generator; dynamic modeling; simulation; transient regime; steady-state

## 1. Introduction

Wind turbines can shut down during operation, typically due to lack of wind, high wind speeds, or need for maintenance, and followed afterward by their transition from rest to operation state. The start-up of medium-large wind turbines is carried out automatically and in a controlled manner, and prior knowledge of their dynamics is typically employed in controllers. Thus, dynamic behavior in transient regimes represents a challenge for researchers and an advantage for designers in the optimization of the control system and wind system design [1–3].

An important issue in approaching the wind system dynamics concerns the assumption of variable wind speed and identification of system dynamic behavior in transient regimes owing to the change in wind speed or starting from rest. Dynamic studies refer to both the wind system as a whole [2–7] and its component subsystems, such as electric generators [8] or mechanical gear transmission [9–11] with the role of speed increasers with

fixed axes [2,12], mobile axes [7,13–17] or combined [18–26]. The overwhelming majority of speed increasers are monomobile (single degree of freedom, 1-DOF) mechanical transmissions [2,16,19,20,23–25,27,28] and rarely differential (2-DOF) transmissions [5,17]. The dynamic response of wind systems can be electrical or mechanical, depending on the type of power pursued: electrical or mechanical power, respectively.

Aiming at improving the performance of electric generators, in conjunction with their overall size reduction, various counter-rotating type generators [2,17,20,29,30] are addressed in literature: with permanent magnets [31], with liquid metals [32], DFIG (Double Fed Induction Generator) that uses a back-to-back Pulse-Width converter Modulation (PWM) for bidirectional control [8], etc.

Dynamic analysis of wind systems and their subsystems requires the use of specific software such as FAST v8.16 (Fatigue, Aerodynamics, Structures, and Turbulence) for aero-elastic dynamic modeling [1,33,34], MATLAB-Simulink [1,2,18,24,35,36], with results having errors below 2% compared to FAST, Ansys 15.0 [15], SIMPACK [33,34] based on dynamic multibody modeling, PSCAD/EMDTC [37], etc. These software packages allow the identification of various representative dynamic parameters related to mechanical efficiency [2,16,38], shaft speeds [3,36,38] and torques [38–40], mechanical powers [3,29,38], and for electrical response: current intensity [36,38] and voltage [38].

Modeling the dynamic response of a wind system requires also knowledge of the mechanical characteristics of both the wind rotor and the electric generator. In literature, these features are modeled as nonlinear [8,27,33] or linear [2,20] functions. Thus, Neagoe et al. [2] addressed the dynamic modeling and simulation of a 10 kW wind turbine with a single wind rotor and counter-rotating generator, equipped with a classical transmission with fixed axes, by considering only one linearized zone of the WR mechanical characteristic: the working zone. The dynamic numerical simulations cover scenarios of wind speed changes during operation by maintaining the operating point on this working zone. However, this research did not consider the starting phase from rest or optimizing the generator's load entry. Similarly, a single linear function for the working zone is proposed for power flow modeling in the steady state of a dual-rotor wind turbine with a counter-rotating generator [20].

In most cases, the dynamic response is an analytical or grapho-analytical result, the most common dynamic modeling methods applied for wind turbines being Newton–Euler [1,2,13,41–43], Lagrange + Runge–Kutta [6,22,28,39,40], lumped parameter theory [10,26,44] or polynomial chaos [12]. Generally, the approaches of WT dynamics consider the gearbox effect in a simplified model by neglecting the rotation of the satellite gears in planetary transmissions.

The dynamic behavior of a wind energy conversion system also depends on the moment when the electric generator is connected to the grid: either from the beginning [2,29,35,45] or at a time after start-up [36,41]. Oyekola et al. [36] stated that synchronous or DC motors can be operated as induction generators if their shaft rotation speed overcomes the synchronous speed. However, this study did not address the optimization problem or the impact of the generator connecting time to the grid on the system's dynamic behavior.

Based on this literature review, the following gaps emerge:

- Choosing an appropriate model of the mechanical characteristics specific to the operating condition of the wind system is still a challenging issue;
- The rotation of the satellite gears from planetary speed increasers is typically neglected;
- The choice of the optimal time for connecting the electric generator to the grid.

Aiming at dealing with these gaps and deepening the understanding of the optimal functioning of a wind system, the present study brings contributions and focuses mainly on the following aspects:

- (a) The dynamic modeling is carried out analytically by applying the Newton–Euler method and the MATLAB-Simulink R2014a software in numerical simulations;
- (b) The functional compatibility of the wind system is ensured by the planetary speed increaser, whose input is connected to the wind rotor, and its two outputs are connected to the generator rotor and stator, respectively;
- (c) The satellite’s own rotation was considered in dynamic modeling by using an equivalent axial moment of inertia;
- (d) The mechanical moments of inertia of the transmission components were reduced at the shafts of the wind rotor and the electric generator;
- (e) The nonlinear mechanical characteristic of the wind rotor is linearized on four zones;
- (f) The dynamic system response is given by a simulation module that allows the generator to connect to the grid after the wind rotor enters the maximum power zone. This simulator also allows the identification of the dynamic behavior of the considered subsystems through specific parameters such as power, torque, speed, and efficiency.

Based on the actual reported results, to the best of our knowledge, the dynamic behavior of this type of wind system with a counter-rotating generator and planetary speed increaser has not been significantly addressed in the literature. Aiming to cover this literature gap, the paper proposes a generalized algorithm for close-form dynamic modeling of single-rotor wind turbine class with planetary speed increaser and counter-rotating generator, patented by authors [46].

The subsequent sections of the paper are organized as follows: Section 2 introduces the conceptual and block diagrams of a counter-rotating wind turbine and formulates the dynamic modeling problem. Section 3 details the proposed generalized algorithm for analytical dynamic modeling. Numerical results for a 100 kW wind turbine are presented and discussed in Section 4, and the paper concludes in Section 5.

## 2. Problem Formulation

Designing wind systems with counter-rotating generators is challenging owing to the branched power flow in planetary transmissions from a single input to dual outputs. The generalized modeling and numerical simulation of the dynamic response of this wind turbine (WT) type is addressed in this paper. Without reducing the generality, a case study of a 1-DOF wind system is considered (Figure 1), consisting of a wind rotor  $R$ , a planetary speed increaser ( $SI$ ) with one input (satellite-carrier  $H$ ) and two outputs (gears 1 and 2) connected to a counter-rotating electric generator  $G$ . The rotor  $GR$  and the stator  $GS$  of the generator are both mobile and rotate in opposite directions.

The block scheme in Figure 1b highlights the interactions between the three key components of the wind system: mechanical power is transmitted from the wind rotor  $R$  via the shaft  $H$  to the speed increaser  $SI$ , which distributes the output power to both the rotor  $GR$  and stator  $GS$ . Obviously, the two power outputs are not independent, the rotor and stator of the generator being permanently characterized in operation by equal and opposite torques (i.e.,  $T_{GS} = -T_{GR}$ ).

The speed increaser is a planetary mechanical transmission with cylindrical gears (1–5, Figure 1), three of which are sun gears (1, 2, and 5  $\equiv$  0), and the solidarized gears 3 and 4 form a double satellite. In practical applications, the planetary transmission includes  $n_s \geq 2$  equiangularly arranged double satellites (3–4).

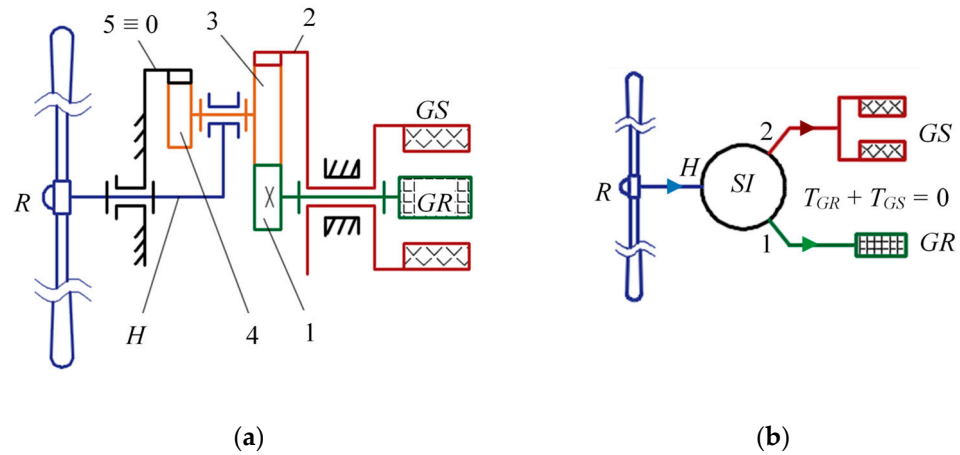


**Figure 1.** Single-rotor wind turbine with counter-rotating electric generator: (a) conceptual scheme; (b) block scheme.

The power input of the speed increaser (i.e., the satellite carrier  $H$ ) is solidarized with the wind rotor  $R$ . Satellites 3–4 engage on the one hand with a fixed ring gear 5 and on the other hand with the sun gear 1, connected with the generator rotor  $GR$ , and with the ring gear 2, coupled to the generator stator  $GS$ . The angular speed of a counter-rotating generator  $G$  ( $\omega_G$ ) is given by the relative speed of the rotor  $GR$  with respect to the stator  $GS$ :

$$\omega_G = \omega_{GR} - \omega_{GS} = \omega_1 - \omega_2. \tag{1}$$

As a result, the kinematic amplification ratios, which describe the transmission of the rotational speed from the wind rotor to the generator rotor ( $i_{a1}$ ) and to the generator stator ( $i_{a2}$ ), respectively, and the total amplification ratio ( $i_{aG}$ ) achieved by the wind turbine, can be established through the following relations:

$$i_{a1} = \frac{\omega_1}{\omega_H}; i_{a2} = \frac{\omega_2}{\omega_H}; i_{aG} = \frac{\omega_1 - \omega_2}{\omega_H} = i_{a1} - i_{a2}, \tag{2}$$

where  $\omega_x$  is the angular velocity of the body  $x = 1, 2, H$ ;  $i_{ay}$ —the amplification ratio from the input  $R$  to the element  $y = 1, 2, G$ .

The dynamic modeling of the analyzed 1-DOF wind system aims to identify its equation of motion  $\varepsilon_R = f(\omega_R, J_x, cst)$ , where  $J_x$  is the mechanical axial moment of inertia of the body  $x = 1, 2, H$ , and  $cst$  represents the set of other constant parameters. The motion of the input shaft (of the wind rotor  $R$ ) is considered as an independent kinematic variable of the wind turbine. By solving this differential equation, the time variation of the torques and kinematic variables (velocities and angular accelerations) related to all system shafts is obtained; the numerical simulations are performed under the assumption of starting the system from rest at a specified constant wind speed.

In the proposed dynamic modeling, the following working premises are considered:

- (1) The rotational elements have geometric symmetry with respect to their own axis of motion, and they are rigid bodies with uniformly distributed mass; as a result, the mass center of a body is located on its own axis of rotation;
- (2) The inertial masses of the mobile elements in the planetary transmission are reduced to their outer shafts; thus, the correlations of the torques in the planetary units coincide with those of static conditions;
- (3) Only the gearing friction losses are considered, neglecting the friction in bearings;
- (4) The pitch angle of WR blades does not change during operation; therefore, the adjustment parameters of the wind rotor remain constant during operation;

- (5) As 1-DOF transmission is employed, the system has one independent motion attributed to the input element, i.e., the wind rotor;
- (6) A direct current (DC) generator is used, and implicitly, its mechanical characteristic is a linear function with constant coefficients; during generator operation, the balancing condition of the torques of the rotor  $GR$  ( $T_{GR}$ ) and of the stator  $GS$  ( $T_{GS}$ ) is described by:  $T_{GR} + T_{GS} = 0$ ;
- (7) The mechanical characteristic of the wind rotor is modeled over four rotational speed intervals by linear functions with constant coefficients, obviously at a constant wind speed.

Dynamic modeling of the WT mechanical system from Figure 1 is based on the block scheme depicted in Figure 2a, in which the planetary speed increaser is modeled by two planetary units (PU) I ( $H$ -5-4-3-1) and II ( $H$ -5-4-3-2), connected in parallel.

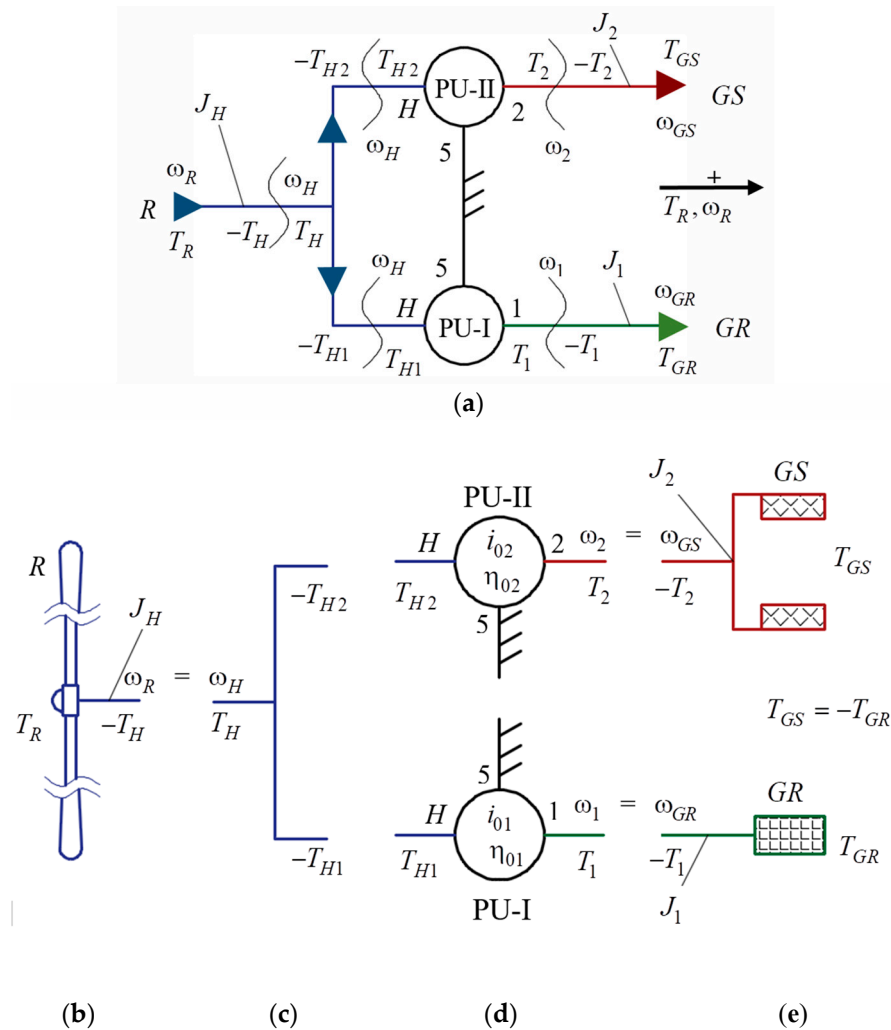


**Figure 2.** (a) Block scheme of the wind turbine and its decomposition into components: (b) wind rotor; (c) intermediate shaft; (d) planetary units; and (e) generator rotor and stator.

By decomposing the wind system from Figure 2a, the six structural components represented in Figure 2b–e are obtained, characterized by specific kinematic and dynamic equations, according to the methodology detailed in Section 3. In the proposed approach, the axial moments of inertia of the components are reduced on the outer shafts of the planetary transmission (i.e., the shafts of the  $R$ ,  $GR$ , and  $GS$  bodies) [37]. Thus, the torque equations for the components in Figure 2c,d can be described by the classical relations established un-

der steady-state conditions and for the other components, depicted in Figure 2b,e,—under dynamic conditions.

The axial moment of inertia of the  $n_s$  satellites 3–4, mounted in parallel, is reduced to the satellite-carrier  $H$  axis based on the principle of equalizing their kinetic energy. The satellite body has a combined rotation (around its own axis) and revolution (around the fixed sun axis) motion; its kinetic energy is considered equal to that of a virtual body with motion around the sun axis having an equivalent moment of inertia  $J_{sH}$ :

$$K_s = \frac{1}{2}n_s \left( m_s v_{Gs}^2 + J_s \omega_s^2 \right) = \frac{1}{2}J_{sH} \omega_H^2, \tag{3}$$

$$J_{sH} = n_s m_s \left( \frac{v_{Gs}}{\omega_H} \right)^2 + n_s J_s \left( \frac{\omega_s}{\omega_H} \right)^2, \tag{4}$$

in which

$$\frac{\omega_s}{\omega_H} = \frac{\omega_H + \omega_{sH}}{\omega_H} = 1 + \frac{\omega_{sH}}{\omega_H} = 1 + \frac{\omega_{sH}}{\omega_{H5}} = 1 - \frac{\omega_{sH}}{\omega_{5H}} = 1 - i_{45}, \quad v_{Gs} = \omega_H \cdot r_H, \tag{5}$$

yielding to

$$J_{sH} = n_s \left( m_s r_H^2 + J_s (1 - i_{45})^2 \right), \tag{6}$$

where  $m_s$  and  $J_s$  are the mass and the axial mechanical moment of a satellite 3–4, respectively ( $J_s$  is established with respect to the own axis of rotation),  $r_H$  is the radius of satellite axis arrangement on the carrier  $H$ , and  $i_{45}$  is the kinematic ratio of the gear pair with fixed axes 4–5 (i.e.,  $i_{45} = z_5/z_4$ , where  $z_4$  and  $z_5$  are the numbers of teeth of gears 4 and 5, respectively).

Next, the main steps of the dynamic modeling algorithm are presented, based on dynamic equations of the transmission external shafts, modeled by the Newton–Euler method, the kinematic and static equations of both planetary units I and II, and the mechanical characteristics of the wind rotor and counter-rotating electric generator.

### 3. Dynamic Modelling

The dynamic equations of the wind system components in the mentioned working premises are linear differential equations of the second order with constant coefficients; they can be obtained by applying the Newton–Euler method considering the positive direction of angular velocity and torque vectors according to Figure 2.

According to premise (2), the following kinematic and static equations can be written for the two planetary units PU-I and PU-II [16], see Figure 2d:

$$\text{PU-I: } \begin{cases} \omega_1 = \omega_H(1 - i_{01}) \\ \omega_H T_{H1} \eta_1 + \omega_1 T_1 = 0 \end{cases} \quad \text{PU-II: } \begin{cases} \omega_2 = \omega_H(1 - i_{02}) \\ \omega_H T_{H2} \eta_2 + \omega_2 T_2 = 0 \end{cases} \tag{7}$$

where  $T_x$  is the resultant torque acting on the element  $x$ ;  $i_{01}$ ,  $i_{02}$ , and  $\eta_1$ ,  $\eta_2$  are the internal kinematic ratio and the efficiency of PU-I and PU-II, respectively, and  $T_H = T_{H1} + T_{H2}$ —Figure 2b.

The relations for the kinematic ratios and transmission efficiencies, specified in Table 1, can be easily derived from Equation (7).

According to the block diagram in Figure 2 and Equation (2), Table 2 illustrates the dynamic schemes of the three WT components, resulting from the decomposition of the wind system into distinctive rigid bodies, as well as their related kinematic and dynamic equations.

**Table 1.** Transmission ratios and efficiencies.

PU	$i_{01,2}$	$i_{a1,2}$	$\eta_{1,2}$
I	$-\frac{z_5}{z_4} \cdot \frac{z_3}{z_1}$	$1 - i_{01}$	$\frac{1 - i_{01}}{1 - i_{01}/\eta_{01}}$
II	$\frac{z_5}{z_4} \cdot \frac{z_3}{z_2}$	$1 - i_{02}$	$\frac{1 - i_{02}}{1 - i_{02}/\eta_{02}}$

$z_j$  is the no. of teeth of the gear  $j = 1 \dots 5$  (see Figure 1);  $\eta_{01}, \eta_{02}$ —internal efficiency of PU-I and PU-II, respectively;  $\eta_{01} = \eta_{02} = \eta_g^2$ , where  $\eta_g$  is the efficiency of a gear pair with fixed axes.

**Table 2.** Schemes and dynamic equations of the WT components.

Body	Dynamic Schemes	Equations
$R \equiv H$ Figure 2a		$\omega_H = \omega_R$ $J_H \varepsilon_H = T_R - T_H$
$1 \equiv GR$ Figure 2e		$\omega_1 = \omega_{GR}$ $\omega_1 = \omega_H \cdot i_{a1}$ $\varepsilon_1 = \varepsilon_H \cdot i_{a1}$ $J_1 \varepsilon_1 = -T_1 + T_{GR}$
$2 \equiv GS$ Figure 2e		$\omega_2 = \omega_{GS}$ $\omega_2 = \omega_H \cdot i_{a2}$ $\varepsilon_2 = \varepsilon_H \cdot i_{a2}$ $J_2 \varepsilon_2 = -T_2 + T_{GS}$

$\varepsilon_x$  is the angular acceleration of the body  $x = 1, 2, H$ ;  $J_H = J_R + J_{shR} + J_{sH}$ ,  $J_1 = J_{g1} + J_{sh1} + J_{GR}$ ,  $J_2 = J_{g2} + J_{sh2} + J_{GS}$ , where g—gear and sh—shaft.

The set of equations in Table 2 is augmented by the linear mechanical characteristics with constant coefficients of the wind rotor (R) and generator (G):

$$T_R = -a_R \omega_R + b_R; T_G = -a_G (\omega_{GR} - \omega_{GS}) + b_G, \tag{8}$$

where  $a_R, b_R, a_G, b_G$  are constant coefficients under steady-state conditions, and by definition  $T_G = T_{GR}$ .

The mechanical characteristic of a wind rotor is a nonlinear function [33,35], which can, however, be acceptably approximated by straight line segments; in this study, four-zone nonlinear characteristic modeling was adopted (Figure 3): zones I and II are used at start-up, zone III includes the point of maximum power  $P_{max}$ , and zones III and IV designate the working zones of the wind rotor. Obviously, the coefficients  $a_R, b_R$  in Equation (8) are replaced specifically by  $a_{Ri}, b_{Ri}, i = 1 \dots 4$  for each of the four zones I...IV.

Obviously, linearizing the WT mechanical characteristic leads to inaccuracies in the calculated torque  $T_R$ , as qualitatively shown in Figure 3. For the case study presented in Section 4, the most significant torque errors are recorded in zone III, with a relative error value of less than 3.4% (its maximum value near the midpoint of zone III, Figure 3), an acceptable level in numerical simulation of such a complex system.

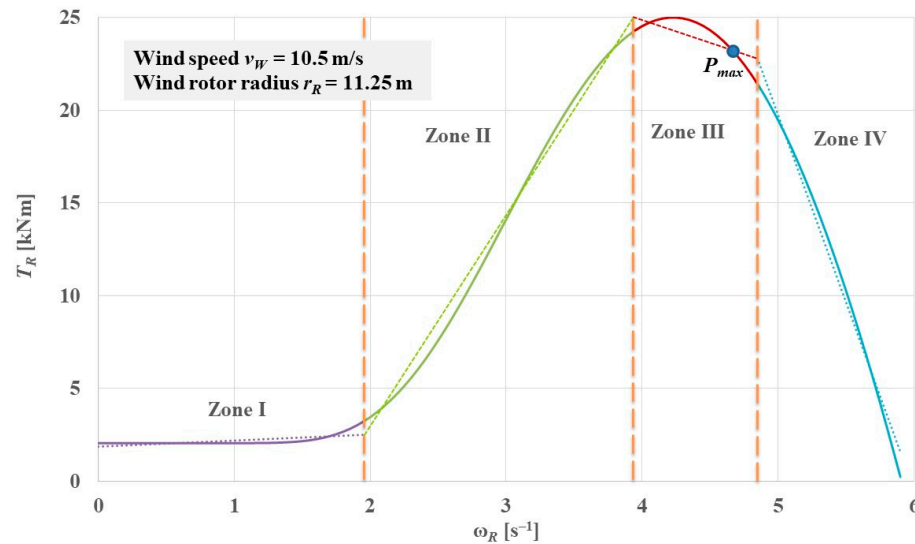


Figure 3. The mechanical characteristic of a wind rotor modeled by four linearized zones.

Substituting the gear ratio and efficiency relations from Table 1 into the kinematic, static, and dynamic equations from Table 2 and corroborating with Rels. (4) and (5), the equation of motion is obtained:

$$\epsilon_R = \frac{\omega_R [a_G (i_{a1} i_{a2} (\eta_1 + \eta_2) - \eta_2 i_{a1}^2 - \eta_1 i_{a2}^2) - a_R \eta_1 \eta_2] + b_G (\eta_2 i_{a1} - \eta_1 i_{a2}) + b_R \eta_1 \eta_2}{J_1 i_{a1}^2 \eta_2 + J_2 i_{a2}^2 \eta_1 + J_H \eta_1 \eta_2}. \quad (9)$$

This equation of motion is a nonhomogeneous second-order differential equation in one variable (independent motion parameter:  $\omega_R$ , where  $\epsilon_R = \frac{d\omega_R}{dt}$ ). This differential equation is solved by numerical integration in MATLAB-Simulink R2014a under known initial conditions: the starting from rest is considered ( $\omega_{R(t=0)} = 0$ ), and the electric machine is coupled to the grid (i.e., the load is activated) when it switches to generator mode ( $\omega_G > \frac{b_G}{a_G}$ ).

The dynamic behavior in a transient regime can be determined by solving the equation of motion (9), obtained using Rels. (7), (8), and Table 2; based on the solution of independent motion, it becomes possible to derive the time evolution of power parameters for all transmission shafts.

### 4. Results and Discussions

Using the previously presented dynamic model, a numerical response is targeted for a 100 kW wind system with parameter values provided in Table 3.

Table 3. Constant intrinsic parameters of the wind system.

$z_i$	$i_0$	$i_a$	$a$ [kNm s] $b$ [kNm]	$\eta$	$J$ [kgm <sup>2</sup> ]
$z_1 = 19$	$i_{01} = -14.8052$ $i_{02} = 2.0837$	$i_{a1} = 15.8052$ $i_{a2} = -1.0837$ $i_{aG} = 16.8889$	$a_{R1} = -0.328, b_{R1} = 1.866$	$\eta_g = 0.9560$ $\eta_1 = 0.9195$ $\eta_2 = 0.8468$	$J_1 = 0.1 \cdot 10^3$ $J_2 = 1 \cdot 10^3$ $J_H = 200 \cdot 10^3$
$z_2 = 135$			$a_{R2} = -11.536, b_{R2} = -20.533$		
$z_3 = 58$			$a_{R3} = 2.298, b_{R3} = 34.014$		
$z_4 = 20$			$a_{R4} = 20.259, b_{R4} = 121.065$		
$z_5 = 97$			$a_G = 0.368, b_G = 27.975$		

The wind turbine has a nominal power of 100 kW, generated by a wind rotor with a diameter of 22.5 m at a nominal wind speed of 10.5 m/s. The start-up of the wind

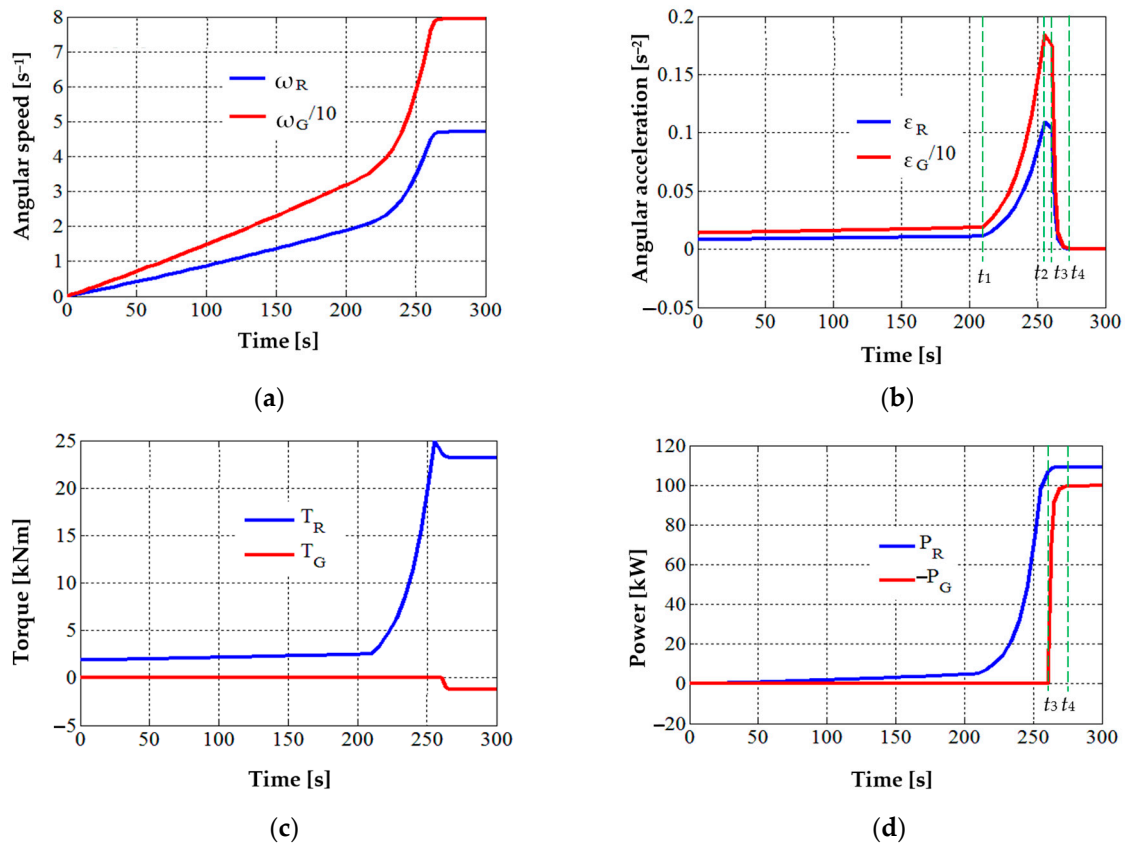
system is performed from rest, and the electric generator load is applied at the time when  $\omega_G = b_G/a_G = 76 \text{ s}^{-1}$ . Thus, the wind system goes through three phases:

- (1) In the first phase, the mechanical energy generated by the wind rotor is used exclusively to overcome inertial resistance (implicitly, to accelerate the system);
- (2) In the second phase, when the generator is coupled to the grid, the generator-resistant torque is added to the inertial load;
- (3) In the third phase, the wind turbine enters into a steady state (i.e., zero accelerations), obtaining the operating point described by the values of the angular velocities and torques, as well as the powers of all the shafts of the wind system, Table 4.

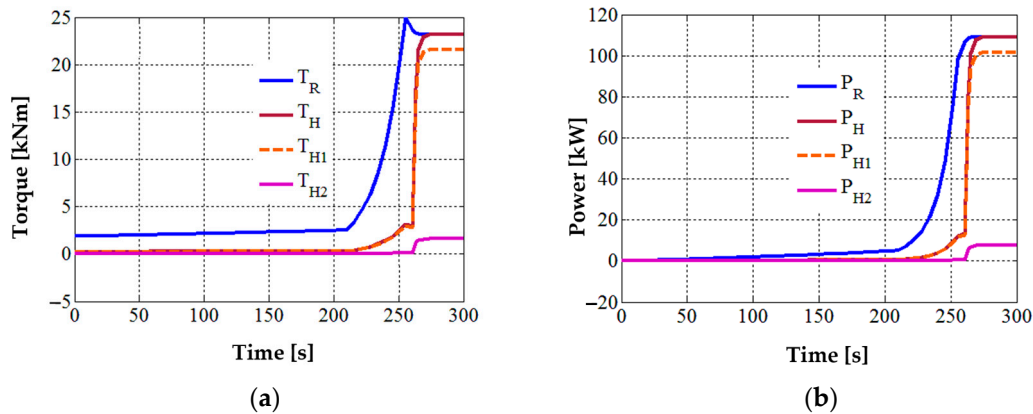
**Table 4.** Operating point of the wind system in steady-state.

Shaft	Torque [kNm]	Angular Speed [s <sup>-1</sup> ]	Power [kW]
R ≡ H	23.208	4.704	109.17
H1	21.600	4.704	101.61
H2	1.608	4.704	7.56
1 ≡ GR	−1.256	74.317	−93.34
2 ≡ GS	1.256	−5.097	−6.40
G	−1.256	79.414	−99.75

The results of the numerical simulation in MATLAB-Simulink R2014a, based on the equation of motion (9) and all the other equations of the analytical model, are depicted in Figures 4–6. The diagrams in these figures highlight the two moments of time delimiting the three phases of the WT transition from rest to steady-state: the electric generator enters the load at  $\approx 260 \text{ s}$ , and the stabilization of the system takes place at  $\approx 280 \text{ s}$  (i.e., the starting time).



**Figure 4.** The wind system dynamic response: (a) input vs. output angular speeds; (b) input vs. output angular accelerations; (c) wind rotor vs. generator torques; (d) wind rotor vs. generator powers.



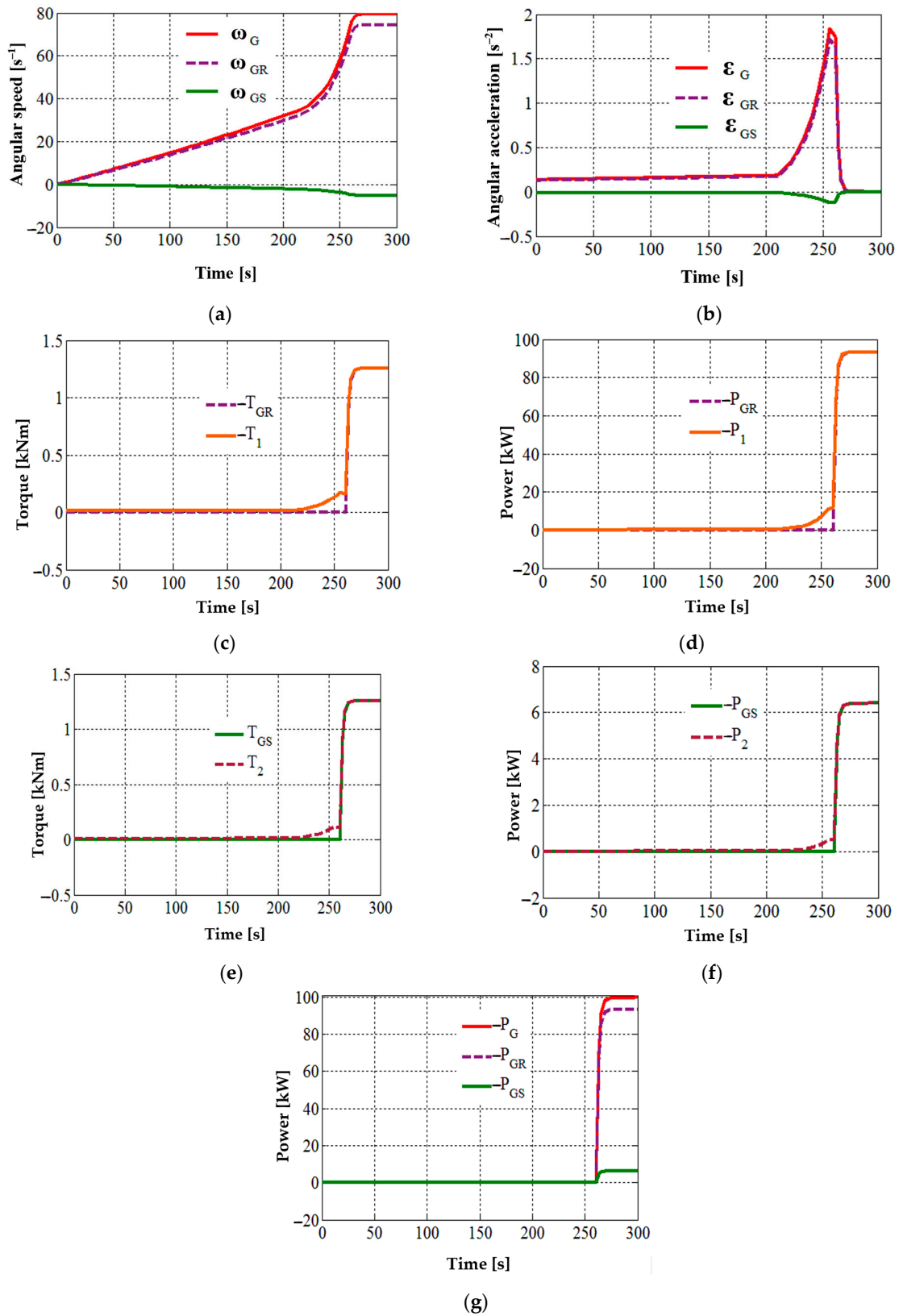
**Figure 5.** The dynamic response at the wind rotor side: (a) wind rotor vs. input torques; (b) wind rotor vs. input powers.

Figure 4 shows comparatively the time variations of the kinematic parameters, torques, and powers from the system input vs. output. Worth noting the quasi-linear variation of all input parameters and output motions in the first part of the start-up phase 1, characterized by  $T_G = 0$  (i.e., the generator runs idle) and wind rotor operation on the zone I (see Figure 3). Since the torque generated by the wind rotor has low values at start-up ( $T_R \approx 2$  kNm, Figure 4c), the system requires a long time ( $\approx 220$  s) of slow increase in speed (Figure 4a) and implicitly in angular acceleration (Figure 4b) as a result of inertial resistance. Once the wind rotor enters zone II (time  $t_1 \approx 220$  s), the system is rapidly accelerated as a result of the greater torque extracted by the wind rotor from the wind. The wind rotor torque reaches its maximum value at the end of zone II (at time  $t_2 \approx 255$  s), followed by a torque decrease into zone III for  $\approx 5$  s. At time  $t_3 \approx 260$  s, the electric generator enters the load (i.e., the wind system goes into phase 2), as the operating conditions of the DC electric machine as a generator are being met:  $\omega_G \geq b_G/a_G = 76$  s $^{-1}$ , Figure 4a. The generator torque increases rapidly up to the value  $T_G = 1.25$  kNm (Figure 4c), with the decrease to zero of the angular acceleration (Figure 4b) and implicitly the entry of the system into steady-state (at time  $t_4 \approx 280$  s).

In phase 3, the generator power stabilizes at  $P_G \approx -100$  kW, the mechanical power extracted from the wind being  $P_R = 109.4$  kW, Figure 4d; implicitly, the transmission efficiency has the value:  $\eta_{WT} = -P_G/P_R = -T_G \cdot \omega_G / (T_R \cdot \omega_R) = 0.9138$ . The efficiency  $\eta_{WT}$  has a value close to the value  $\eta_1$  and is significantly higher than  $\eta_2$  (see Table 3); thus, the advantage of power branching in complex mechanisms compared to the serial connection of component mechanisms is also well emphasized.

Figure 5 shows the distribution of torques and mechanical power on the inputs of planetary units I and II, as well as the influence of inertia on the WT dynamic behavior. In the first part of phase 1, a significant difference between the driving torque  $T_R$  and the resistant torque  $T_H$  is noted (Figures 2 and 5a). This fact is owing to the insignificant values of the torques  $T_{H1}$  and  $T_{H2}$ , also caused by the reduced inertial resistances of the output shafts (the values of the moments of inertia  $J_1$  and  $J_2$  being much lower compared to  $J_H$ :  $J_H \approx 2000 \cdot J_1 \approx 200 \cdot J_2$ , see Figure 2, Tables 2 and 3); this reduced inertial effect of the output shafts is also confirmed by their relatively reduced values of angular accelerations. As a result, the torque  $T_R$  is mostly used to overcome the inertial load of the input shaft  $H$ . Once the generator enters the load, the  $T_{H1}$  torque increases much faster than  $T_{H2}$ , becoming the major component of  $T_H$  in the steady state. Although the GR rotor and GS stator torques are equal in steady-state, the significant difference between  $T_{H1}$  and  $T_{H2}$  is explained by the large differences in the amplification ratios  $i_{a1} = 15.8052$  and  $i_{a2} = -1.0837$  (see Table 3) corresponding to the two power branches. The power variation on the input shafts (Figure 5b) follows a similar evolution as the input torques (Figure 5a): most of the

wind rotor power (over 93%) is directed to the planetary unit I and, implicitly, to the GR rotor—the body with the highest rotation speed.



**Figure 6.** The dynamic response at the generator side: (a) generator angular speeds; (b) generator angular accelerations; (c) generator rotor vs. output 1 torques; (d) generator rotor vs. output 1 powers; (e) generator stator vs. output 2 torques; (f) generator stator vs. output 2 powers; (g) mechanical powers.

Figure 6 illustrates the WT dynamic behavior at the output side, characterized by the branched power transmission via the rotor  $GR$  and the stator  $GS$ , respectively; the contribution of the mobile stator to the overall performance of the wind system is particularly highlighted. The output angular speeds and accelerations (Figure 6a,b) have a linear dependence on the independent motion of the wind rotor; according to the relations in Table 2, they follow the variation profile of the angular velocity  $\omega_R$  and acceleration  $\varepsilon_R$ , respectively (Figure 4a,b), with values amplified with the ratios  $i_{a1}$ ,  $i_{a2}$ , and  $i_{aG}$ , respectively. Note the much lower speed and acceleration of the  $GS$  stator compared to the  $GR$  rotor, and finally, the smaller power contribution from the  $GS$  stator vs.  $GR$  rotor due to the large inequality:  $|i_{a2}| \ll |i_{a1}|$ . Obviously, this situation can be improved by optimizing the ratio between  $i_{a2}$  and  $i_{a1}$ , as well as the large ratio between the inertia of the  $GS$  stator and the  $GR$  rotor.

At the time the generator enters the load ( $\approx 260$  s), the torques  $T_1$  (Figure 6c) and  $T_2$  (Figure 6e), respectively, the powers  $P_1$  (Figure 6d) and  $P_2$  (Figure 6f) reflect the inertial impact of the output shafts (1 and 2). Although the two shafts have different moments of inertia ( $J_2 = 10J_1$ , see Table 3), the large acceleration difference in favor of shaft 1  $\equiv GR$  makes the inertial resistance of shaft 1 greater than that of shaft 2 (maximum 0.172 vs. 0.118 kNm) in phase (1). In steady-state, the high angular velocity of the  $GR$  rotor allows it to receive a much higher power compared to the  $GS$  stator (i.e.,  $|P_{GR}| = 93.34$  kW  $>$   $|P_{GS}| = 6.40$  kW). Thus, the power contribution of the  $GS$  stator to the total power of the generator is  $\sim 6.4\%$  (Figure 6g), the largest share of the power flow being distributed to the  $GR$  rotor.

The results of the dynamic numerical simulations, based on the analytical dynamic model developed in this study, allow the identification of the WT dynamic behavior in the transient regime during starting-up from rest, as well as the values of the operating point parameters in steady-state.

## 5. Conclusions

The paper proposes a generalized algorithm for dynamic modeling of the wind system class of type: single-rotor, 1-DOF planetary transmission, and counter-rotating generator.

The counter-rotating generator requires a dual-output speed increaser, leading to a branched power flow configuration where the input power is distributed to the two parallel-connected planetary units. The analytical equation of motion is derived by combining the dynamic equations of the shafts, the mechanical characteristics of the wind rotor and electric generator, and the kinematic and static equations of the planetary gear transmission, which together describe the complex interactions within this system. This system of equations allows the analytical establishment of the wind system equation of motion and implicitly its operating point by numerical solution in transient mode and in steady-state.

The analytical study and the results of the numerical simulations carried out on a case study of a wind turbine with a rated power of 100 kW allowed us to draw the following conclusions:

- The proposed generalized modeling algorithm allows obtaining analytically the equation of motion of the wind system, formulated as a nonhomogeneous differential equation of the second order in a single independent variable, describing the wind rotor motion;
- By numerically solving the equation of motion, using the MATLAB-Simulink R2014a software, the dynamic response of the wind system in transient mode and the operating point in steady-state are obtained;
- The analysis of the dynamic response in transient mode, when starting from rest at constant wind speed, allowed the identification of the starting time of the wind system,

as well as the stresses induced by the inertial load alone and by its combination with the generator load;

- Unlike the case of traditional wind turbines, equipped with a conventional generator with a fixed stator, the counter-rotating generator allows an additional input of power brought by the mobile stator GS; in the analyzed case, the additional power supply by GS in steady-state is ~6.4%.

The proposed generalized algorithm can be applied, with rigorous adaptations, to other types of wind systems, regardless of their complexity: with one or more wind rotors, with conventional or counter-rotating electric generators, with fixed-axis or planetary speed increaser. Likewise, the developed MATLAB-Simulink R2014a model can also be applied iteratively for the purpose of constructive-functional optimization of this particular type of wind system, as well as in the simulation scenarios of variable operational conditions determined by the change in wind speed.

The authors intend to address in the future the dynamic optimization of such wind systems and the validation of theoretical results through the experimental research of some functional models on specialized testing rigs.

## 6. Patents

Saulescu, R., Neagoe, M., Visa, M., Jaliu, C., Munteanu, O., Totu, I. Cretescu, N. Monomobile planetary speed increaser with two counter-rotating outputs, Patent no RO 131740 B1, 29 November 2023.

**Author Contributions:** Conceptualization, M.N. and R.S.; methodology, M.N. and R.S.; software, R.S. and M.N.; validation, M.N. and R.S.; formal analysis, M.N. and R.S.; investigation, R.S. and M.N.; resources, R.S. and M.N.; data curation, M.N. and R.S.; writing—original draft preparation, M.N. and R.S.; writing—review and editing, M.N.; visualization, R.S.; supervision, M.N. All authors have read and agreed to the published version of the manuscript.

**Funding:** This research received no external funding.

**Institutional Review Board Statement:** Not applicable.

**Informed Consent Statement:** Not applicable.

**Data Availability Statement:** The original contributions presented in this study are included in the article. Further inquiries can be directed to the corresponding author.

**Conflicts of Interest:** The authors declare no conflict of interest.

## Nomenclature

$a_G$	speed coefficient in the generator mechanical characteristic
$a_R$	speed coefficient in the wind rotor mechanical characteristic
$b_G$	torque term in the generator mechanical characteristic
$b_R$	torque term in the wind rotor mechanical characteristic
$DOF$	degree of freedom
$DC$	direct current
$DFIG$	double fed induction generator
$FAST$	fatigue, aerodynamics, structures, and turbulence
$g$	gear
$G$	electric generator
$GR$	generator rotor
$GS$	generator stator
$H$	satellite carrier
$i$	kinematic ratio

$i_0$	internal kinematic ratio
$i_a$	speed amplification ratio
$J$	mechanical axial moment of inertia
$K_s$	kinetic energy
$m$	mass
$n_s$	number of satellites
$P$	power
$PWM$	pulse-width converter modulation
$PU$	planetary unit
$r$	radius
$R$	wind rotor
$t$	time
$T$	torque
$\eta$	efficiency
$\eta_0$	internal efficiency
$\eta_g$	efficiency of a gear pair
$\omega$	angular speed
$\varepsilon$	angular acceleration
$SI$	speed increaser
$sh$	shaft
$v$	linear speed
$WR$	wind rotor
$WT$	wind turbine
$z_j$	number of teeth of gear $j$

## References

1. Cottura, L.; Caradonna, R.; Ghigo, A.; Novo, R.; Bracco, G.; Mattiazzo, G. Dynamic Modeling of an Offshore Floating Wind Turbine for Application in the Mediterranean Sea. *Energies* **2021**, *14*, 248. [\[CrossRef\]](#)
2. Neagoe, M.; Saulescu, R.; Jaliu, C.; Neagoe, I. Dynamic Analysis of a Single-Rotor Wind Turbine with Counter-Rotating Electric Generator under Variable Wind Speed. *Appl. Sci.* **2021**, *11*, 8834. [\[CrossRef\]](#)
3. Sanchez, R.; Medina, A. Wind turbine model simulation: A bond graph approach. *Simul. Model. Pract. Theory* **2014**, *41*, 28–45. [\[CrossRef\]](#)
4. Al-Hamadani, H.; An, T.; King, M.; Long, H. System Dynamic Modelling of Three Different Wind Turbine Gearbox Designs under Transient Loading Conditions. *Int. J. Precis. Eng. Manuf.* **2017**, *18*, 11. [\[CrossRef\]](#)
5. Lin, A.-D.; Hung, T.-P.; Kuang, J.-H.; Tsai, H.-A. Power Flow Analysis on the Dual Input Transmission Mechanism of Small Wind Turbine Systems. *Appl. Sci.* **2020**, *10*, 7333. [\[CrossRef\]](#)
6. Rubio, J.J.; Soriano, L.A.; Yu, W. Dynamic Model of a Wind Turbine for the Electric Energy Generation. *Math. Probl. Eng.* **2014**, *2014*, 409268. [\[CrossRef\]](#)
7. Wang, B.; Michon, M.; Holehouse, R.; Atallah, K. Dynamic Behaviour of a Multi-MW Wind Turbine. In Proceedings of the IEEE Energy Conversion Congress and Exposition (ECCE), Montreal, QC, Canada, 20–24 September 2015; ISBN 978-1-4673-7151-3.
8. Abo-Khalil, A.; Alyami, S.; Sayed, K.; Alhejji, A. Dynamic Modeling of Wind Turbines Based on Estimated Wind Speed under Turbulent Conditions. *Energy* **2019**, *12*, 1907. [\[CrossRef\]](#)
9. Dewangan, P.; Parey, A.; Hammami, A.; Chaari, F.; Haddar, M. Dynamic characteristics of a wind turbine gearbox with amplitude modulation and gravity effect: Theoretical and experimental investigation. *Mech. Mach. Theory* **2022**, *167*, 104468. [\[CrossRef\]](#)
10. Dong, H.; Zhang, C.; Wang, D.; Xu, S. Dynamic characteristics of gear box with PGT for wind turbine. *Procedia Comput. Sci.* **2017**, *109*, 801–808. [\[CrossRef\]](#)
11. Fan, Z.; Zhu, C.; Li, X.; Liang, C. The transmission characteristic for the improved wind turbine gearbox. *Energy Sci. Eng.* **2019**, *7*, 1368–1378. [\[CrossRef\]](#)
12. Mabrouk, I.B.; Hami, A.E.; Walha, L.; Zghal, B.; Haddar, M. Dynamic response analysis of Vertical Axis Wind Turbine geared transmission system with uncertainty. *Eng. Struct.* **2017**, *139*, 170–179. [\[CrossRef\]](#)
13. Li, D.; Zhao, Y. A dynamic-model-based fault diagnosis method for a wind turbine planetary gearbox using a deep learning network. *Prot. Control. Mod. Power Syst.* **2022**, *7*, 22. [\[CrossRef\]](#)
14. Mathis, R.; Rémond, Y. Kinematic and dynamic simulation of epicyclic gear trains. *Mech. Mach. Theory* **2009**, *44*, 412–424. [\[CrossRef\]](#)

15. Mohsine, A.; Mostapha, B.E.; Alaoui, R.E.; Daoudi, K. Comparative Study in the Structural and Modal Analysis of a Wind Turbine Planetary Gear Based on Material Reduction Criteria Using FEM. *Int. J. Renew. Energy Res.* **2019**, *9*, 2. [CrossRef]
16. Neagoe, M.; Saulescu, R.; Jaliu, C.; Simionescu, P.A. A Generalized Approach to the Steady-State Efficiency Analysis of Torque-Adding Transmissions Used in Renewable Energy Systems. *Energies* **2020**, *13*, 4568. [CrossRef]
17. Saulescu, R.; Neagoe, M.; Jaliu, C.; Munteanu, O. A Comparative Performance Analysis of Counter-Rotating Dual-Rotor Wind Turbines with Speed-Adding Increases. *Energies* **2021**, *14*, 2594. [CrossRef]
18. Girsang, I.P.; Dhupia, S.J.; Muljadi, E.; Singh, M.; Pao, Y.P. Gearbox and Drivetrain Models to Study Dynamic Effects of Modern Wind Turbines. *IEEE Trans. Ind. Appl.* **2013**, *50*, 3777–3786. [CrossRef]
19. Li, Z.; Wen, B.; Peng, Z.; Dong, X.; Qu, Y. Dynamic modeling and analysis of wind turbine drivetrain considering the effects of non-torque loads. *Appl. Math. Model.* **2020**, *83*, 146–168. [CrossRef]
20. Neagoe, M.; Saulescu, R.; Jaliu, C. Design and Simulation of a 1 DOF Planetary Speed Increaser for Counter-Rotating Wind Turbines with Counter-Rotating Electric Generators. *Energies* **2019**, *12*, 1754. [CrossRef]
21. Nejad, A.R.; Guo, Y.; Gao, Z.; Moan, T. Development of a 5 MW Reference Gearbox for Offshore Wind Turbines. *Wind Energy* **2016**, *9*, 6. [CrossRef]
22. Ren, Z.; Zhou, S.; Wen, B. Dynamic coupled vibration analysis of a large wind turbine gearbox transmission system. *J. Vibroengineering* **2015**, *7*, 6.
23. Shi, W.; Kim, C.-W.; Chung, C.-W.; Park, H.-C. Dynamic Modeling and Analysis of a Wind Turbine Drivetrain Using the Torsional Dynamic Model. *Int. J. Precis. Eng. Manuf.* **2012**, *14*, 153–159. [CrossRef]
24. Shi, W.; Ning, D.; Ma, Z.; Ren, N.; Park, H. Parametric Study of Drivetrain Dynamics of a Wind Turbine Using the Multibody Dynamics. *Int. J. Mech. Eng. Appl.* **2019**, *7*, 2. [CrossRef]
25. Shi, W.; Park, H.-C.; Na, S.; Song, J.; Ma, S.; Kim, C.-W. Dynamic Analysis of Three-Dimensional Drivetrain System of Wind Turbine. *Int. J. Precis. Eng. Manuf.* **2014**, *15*, 7. [CrossRef]
26. Wang, J.; Yang, S.; Liu, Y.; Mo, R. Analysis of Load-Sharing Behavior of the Multistage Planetary Gear Train Used in Wind Generators: Effects of Random Wind Load. *Appl. Sci.* **2019**, *9*, 5501. [CrossRef]
27. Farias, M.G.; Galhardo, A.B.M.; Vaz, R.P.J.; Pinho, T.J. A steady-state based model applied to small wind turbines. *J. Braz. Soc. Mech. Sci. Eng.* **2019**, *41*, 209. [CrossRef]
28. Xiang, L.; Gao, N.; Hu, A. Dynamic analysis of a planetary gear system with multiple nonlinear parameters. *J. Comput. Appl. Math.* **2017**, *327*, 325–340. [CrossRef]
29. Erturk, E.; Sivrioglu, S.; Bolat, F.C. Analysis Model of a Small Scale Counter-Rotating Dual Rotor Wind Turbine with Double Rotational Generator Armature. *Int. J. Renew. Energy Res.* **2018**, *8*, 4. [CrossRef]
30. Wrobel, R.; Drury, D.; Mellor, P.D.; Booker, J.D. Contra-Rotating Modular Wound Permanent Magnet Generator for a Wind Turbine. In Proceedings of the 2008 4th IET Conference on Power Electronics, Machines and Drives (PEMD 2008), York, UK, 2–4 April 2008; pp. 330–334. [CrossRef]
31. Booker, J.D.; Mellor, P.H.; Wrobel, R.; Drury, D. A compact, high efficiency contra-rotating generator suitable for wind turbines in the urban environment. *Renew. Energy* **2010**, *35*, 2027–2033. [CrossRef]
32. Egorov, A.V.; Kaizer, Y.F.; Lysyannikov, A.V.; Kuznetsov, A.V.; Shram, V.G.; Pavlov, A.I.; Smirnov, M.Y.; Kuznetsova, P.A. Counter-rotating electric generator for wind power plants with liquid metal energy transfer. *J. Phys. Conf. Ser.* **2021**, *2094*, 052018. [CrossRef]
33. Dong, W.; Xing, Y.; Moan, T. Time Domain Modeling and Analysis of Dynamic Gear Contact Force in a Wind Turbine Gearbox with Respect to Fatigue Assessment. *Energies* **2012**, *5*, 4350–4371. [CrossRef]
34. Xing, Y.; Guo, Y.; Keller, J.; Moan, T. Model Fidelity Study of Dynamic Transient Loads in a Wind Turbine Gearbox. In Proceedings of the WINDPOWER Conference 2013, Chicago, IL, USA, 5–8 May 2013. Available online: <https://www.osti.gov/biblio/1078065> (accessed on 7 October 2024).
35. Jansuya, P.; Kumsuwan, Y. Design of MATLAB/Simulink Modeling of Fixed-pitch Angle Wind Turbine Simulator. *Energy Procedia* **2013**, *34*, 362–370. [CrossRef]
36. Oyekola, P.; Mohamed, A.; Pumwa, J. Renewable Energy: Dynamic Modelling of a Wind Turbine. *Int. J. Innov. Technol. Explor. Eng.* **2019**, *9*, 9. [CrossRef]
37. Santoso, S.; Le, H. Fundamental time-domain wind turbine models for wind power studies. *Renew. Energy* **2007**, *32*, 2436–2452. [CrossRef]
38. Teixeira, M.R.; Ohara, M.F.; Milhomens, D.M.; de Paula, S.A. Dynamical Behavior of a Wind Turbine Power Train Considering a Rotor-Gearbox-Generator Coupled Model. In Proceedings of the 6th ECCOMAS Thematic Conference on Computational Methods in Structural Dynamics and Earthquake Engineering, Rhodes Island, Greece, 15–17 June 2017; pp. 3543–3555. [CrossRef]
39. Park, Y.; Shi, W.; Park, H. Effect of the Variable Gear Mesh Model in Dynamic Simulation of a Drive Train in the Wind Turbine. *Eng. Rev.* **2020**, *41*, 113–124. [CrossRef]

40. Park, Y.; Park, H.; Ma, Z.; You, J.; Shi, W. Multibody Dynamic Analysis of a Wind Turbine Drivetrain in Consideration of the Shaft Bending Effect and a Variable Gear Mesh Including Eccentricity and Nacelle Movement. *Front. Energy Res.* **2021**, *8*, 604414. [[CrossRef](#)]
41. Fernández, M.L.; Saenz, J.R.; Jurado, F. Dynamic models of wind farms with fixed speed wind turbines. *Renew. Energy* **2006**, *31*, 1203–1230. [[CrossRef](#)]
42. Song, Z.; Shi, T.; Xia, C.; Chen, W. A novel adaptive control scheme for dynamic performance improvement of DFIG-Based wind turbines. *Energy* **2012**, *38*, 104–117. [[CrossRef](#)]
43. Zhao, M.; Ji, J. Dynamic Analysis of Wind Turbine Gearbox Components. *Energies* **2016**, *9*, 110. [[CrossRef](#)]
44. Zhu, C.; Xu, X.; Liu, H.; Luo, T.; Zhai, H. Research on dynamical characteristics of wind turbine gearboxes with flexible pins. *Renew. Energy* **2014**, *68*, 724–732. [[CrossRef](#)]
45. Yi, P.; Zhang, C.; Guo, L.; Shi, T. Dynamic modeling and analysis of load sharing characteristics of wind turbine gearbox. *Adv. Mech. Eng.* **2015**, *7*, 3. [[CrossRef](#)]
46. Saulescu, R.; Neagoe, M.; Visa, M.; Jaliu, C.; Munteanu, O.; Totu, I.; Cretescu, N. Monomobile Planetary Speed Increaser with Two Counter-Rotating Outputs. RO 131740 B1, 29 November 2023.

**Disclaimer/Publisher’s Note:** The statements, opinions and data contained in all publications are solely those of the individual author(s) and contributor(s) and not of MDPI and/or the editor(s). MDPI and/or the editor(s) disclaim responsibility for any injury to people or property resulting from any ideas, methods, instructions or products referred to in the content.